RADAR INVESTIGATIONS OF SUBSURFACE ICE AT ASKJA VOLCANO, NORTHERN ICELAND.

D. M. H. Baker[1], E. S. Shoemaker[3], J. A. Richardson[1,2], S. P. Scheidt[1,4], P. L. Whelley[1,2], L. M. Carter[3], K. E. Young[1]. [1]Solar System Exploration Division, NASA Goddard Space Flight Center, Greenbelt, MD 20771 (david.m.hollibaughbaker@nasa.gov), [2]Dept. of Astronomy, Univ. of Maryland, College Park, MD 20742, [3]Lunar and Planetary Laboratory, Univ. of Arizona, Tucson, AZ 85721, [4]Dept. of Physics and Astronomy, Howard University, Washington, D.C. 20059.

Introduction: Locating and characterizing buried water ice in the shallow (0–10 m) subsurface of the Moon and Mars is important for addressing both science and human exploration objectives [1,2]. The spatial and vertical distribution of subsurface water ice can be characterized by geophysical techniques, such as orbital Synthetic Aperture Radar (SAR) or ground-penetrating radar (GPR). These technologies are expected to make important contributions to our understanding of planetary subsurface ice in the coming decades. For example, the Mars Ice Mapper mission concept planned for development [3] would carry an L-band SAR to search for subsurface ice at possible human landing sites in the mid-latitudes of Mars. To assist in the interpretation of these future radar datasets, we conducted analog field GPR investigations of buried ice within the Askja Caldera, Iceland and use these to inform airborne L-band SAR data.

Field Analog Site. Buried ice layers were formed within the caldera of the Askja central volcano (Northern Iceland, Fig. 1) when eruptions in March, 1875 [4] and October to November, 1961 [5] deposited pyroclasts on fresh snowfall. This snowfall then densified into solid ice, likely through a combination of compaction, meltwater refreeze and ice aggradation, and has remained insulated since each eruption. Today, ice deposits are located under decimeter to meters of pumice ("1875 pumice") and basaltic ash and lapilli ("1961 scoria").

Methodology: *GPR.* Fifty surveys over pyroclasts were performed using shielded GSSI GPR antennae at 200 and 400 MHz. Radar traces were recorded at a rate of 100/m, triggered with a wheel odometer, and a mounted GPS was used for geopositioning. GPR data were then processed in RADAN 7 and readgssi software using standard techniques. Attenuation analysis was performed by computing an average trace across subsections of each radargram and fitting a second-order polynomial or linear model to the trace. Models for geometric spreading and scattering losses were applied based on the methods of previous work [6].

Borings and trenches. A rotary hammer drill and a 2–3/8-inch core auger were used at 11 borehole sites along GPR transects to sample subsurface materials in 15–30 cm increments down to 1.6 m. Trenches were also dug to validate GPR analysis results.

Aerial surveys. An orthoimage mosaic and a Digital Elevation Model (DEM) were produced for the study area (Fig. 1) using a Mavic 2 Pro quadcopter. Images collected by the quadcopter were processed using AgiSoft Metashape software.

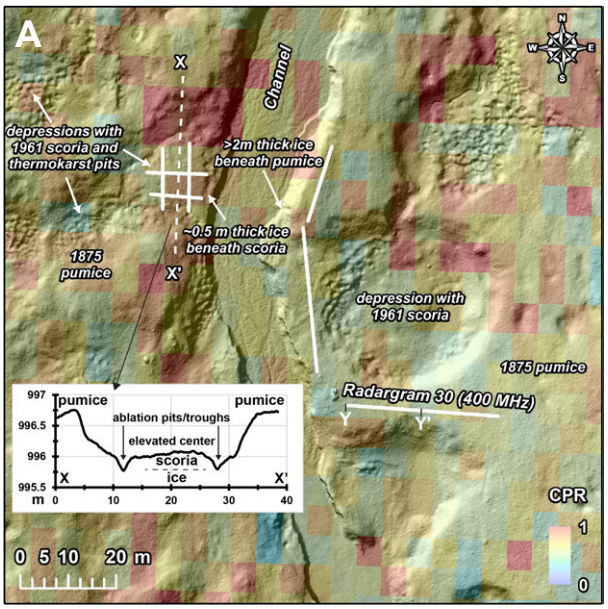

Fig. 1. (A) Portion of study area with UAV DEM hillshade overlain by UAVSAR L-band CPR values. White solid lines are GPR transects. Dashed line locates the inset topographic profile of ice-rich depression with 1961 scoria and edge ablation troughs. (B) Location of panel A within the Askja caldera (Google Earth, Aug. 2020).

SAR: We used UAVSAR polarimetric L-band (1.26 GHz) data collected in May 2015 at 5x6 m/pixel resolution. Ground-projected complex cross product data were used to calculate the Circular Polarization Ratio (CPR) [e.g., 7], which is a common product for assessing ice and roughness characteristics on planetary bodies [8]. The L-band frequency enables assessment of subsurface properties in the top ~2-3 meters.

Results and Interpretations: Our field observations reveal widespread, massive buried ice residing at depths of 30-50 cm below the surface, extending spatially to many tens of meters within the Askja caldera and on the flanks. Distinct ice layers up to 0.5 to >2 m in thickness are located beneath both 1961 ash and lapilli and 1875 pumice. Many are tied to permafrost and thermokarst landforms (Fig. 1A)

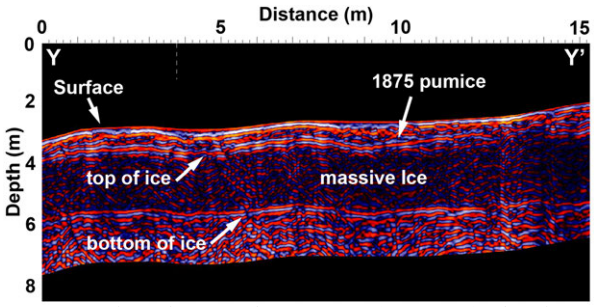

Fig. 2. Portion of GPR radargram #30 (400 MHz), showing radar power with applied three-point gain and terrain correction. Continuous reflections are shown at the surface, the interface of 1875 pumice and ice, and the base of the ice. Depths (vertical axis) assume a dielectric constant of 4.0.

GPR Stratigraphy: Distinct, continuous reflectors are observed in both 200 and 400 MHz GPR data that we interpret as interfaces between dry pyroclasts and frozen deposits with a water ice matrix and between frozen deposits and pure ice (Fig. 2). Strong reflectors occur at both the top of the ice table (~0.5-1 m depth) and at the base of the ice deposits. Some enhancement of the dielectric contrast and returned power may result from meltwater residing along these interfaces. We confirmed the stratigraphy with coordinated bore holes.

GPR Attenuation: As expected for homogenous ice deposits, GPR radargrams show relatively little backscattering within ice layers compared with the pyroclastic layers (Fig. 2). The overall attenuation properties, including two-way loss rate of ~6-7 dB/m of the ice (Fig. 3A) are similar to other permafrost regions [e.g., 6]. The character of the attenuation is different for non-ice regions such as pumice-covered lava flows located near the study area, which is more linear and have higher loss rates of 10 dB/m (Fig. 3B).

Aerial UAV and topography: UAV orthophotos and DEMs reveal widespread thermokarst landforms (Fig. 1). Many ice-rich areas have raised centers and edge troughs and pits with enhanced ablation (Fig. 1A, inset). This topographic signature is interpreted to be the result of ice aggradation and soil heave processes that occur for other permafrost landforms [9].

L-band SAR: UAVSAR data show moderate to high CPR values in our study area (average and standard deviation of 0.5 +/- 0.22 over 250x250 m area) (Fig. 1A). Preliminary analysis suggest similarities in values to the surfaces of nearby lava flows (1961 and 2014 Holuhraun), even in relatively flat areas within the caldera. For the flat areas, the elevated CPR values could be a product of subsurface roughness/blocks from buried lava flows, or could be an enhancement due to buried ice in the subsurface. We are assessing these scenarios in context of our GPR and field observations.

Discussion and implications for ice detection on the Moon and Mars: GPR data at our analog site reveals the ability of GPR to detect shallow layers of regolith (pyroclasts here) and massive ice within a few meters of the surface. The 400 MHz attenuation properties are also different between ice and non-ice areas providing another means of identifying subsurface ice. We are in the process of better quantifying these attenuation properties. Assessing SAR data for buried ice layers is challenging over topographically rough areas modified by thermokarst processes and when ice layers are spatially small compared with the radar resolution. Similar challenges are expected for the analysis of SAR over pitted and thermokarst terrains on Mars. Evaluation of further decomposition techniques will aid future SAR interpretations.

Acknowledgments: This work was supported by the Goddard Instrument Field Team and was a part of the 2019 Volcanic Deposit Evolution and Origins (VIDEO) expedition. We thank the Vatnajökull National Park for their support and permission to carry out this work.

References: [1] MEPAG ICE-SAG Final Report (2019) http://mepag.nasa.gov/reports.cfm. [2] LEAG (2016) The Lunar Exploration Roadmap, https://www.lpi.usra.edu/leag/roadmap/. [3] Watzin J. and Haltigin, T. (2020) Mars Exploration Ice Mapper, presented at April 2020 MEPAG meeting, https://mepag.jpl.nasa.gov/meetings.cfm. [4] Carey R. J. et al. (2010) *Bull. Volc.*, 72(3), 259–278. [5] Thorarinsson, S. and Sigvaldason, G. E. (1962) *Am. J. Sci.,* 260, 641–651. [6] Boisson, J. et al. (2011) *J. Geophys. Res.* 116, E11003. [7] Neish, C.D. et al. (2017) *Icarus* 281, 73–89. [8] Campbell, B.A. (2012) *J. Geophys. Res.* 117, E06008. [9] Camels, F. et al. (2008) *Geomorphology* 97, 287–299.

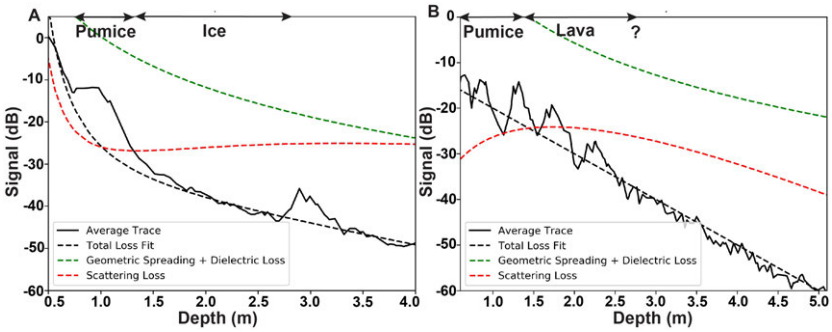

Fig. 3. Average 400 MHz GPR traces (solid black lines) from portion of radargram #30 (see Fig. 2) with ice layers (A) and from an ice-free 1961 lava flow covered by 1 m of pumice (B). Black dashed lines are second-order polynomial (A) and linear (B) fits to the traces. Green and red dashed lines show radar loss models described in [6].